www.czasopisma.pan.pl PAN POLSKA AKADEMIA NAUK www.journals.pan.pl

Arch. Metall. Mater. **68** (2023), 1, 249-255

DOI: https://doi.org/10.24425/amm.2023.141501

ENRIQUE ROCHA-RANGEL[1*], CARLOS A. CALLES-ARRIAGA[1],
JUAN LÓPEZ-HERNÁNDEZ[1], JOSÉ A. RODRÍGUEZ-GARCÍA[1]

MANUFACTURE OF TOUGHENED Al_2O_3-BASED COMPOSITES BY THE COMBINATION OF RBAO AND SPS PROCESSES

The effect of additions of silver or titanium (0.5 or 3 vol.%) microparticles on the microstructure, as well as some physical properties of Al_2O_3-based composites, were studied. The processing method for the manufacturing of alumina-based composites was a combination of RBAO and SPS processes. After the SPS process, bodies with almost full density were obtained. Observations by optical microscopy show a very fine and homogenous microstructure in all samples. Concerning mechanical properties, the addition of metals on alumina increases its fracture toughness significantly (112% for the sample with additions of silver, while the composite with additions of titanium fracture toughness increases by 72%). In terms of optical properties, both silver and titanium improve the absorbance in the visible range.

Keywords: RBAO process; SPS process; Al_2O_3; Fracture toughness; Ceramic composites

1. Introduction

Because alumina has a hexagonal crystalline structure with an ionic-covalent bond, it presents excellent physical, dielectric, and mechanical properties; it also has good corrosion resistance, as well as high chemical and thermal stability at high temperatures. For these reasons, alumina is used in the textile industry for yarn guides, in nozzles for flaming or just throwing sparks, in uses of melting pots, as refractory lining of furnaces, protectors for thermocouples, in electronics it is used in components for interconnection, as cutting tools and it is also used as a biomaterial because it is inert and insoluble [1]. However, despite its remarkable characteristics, its low fracture toughness value limits many other potential applications since slight imperfections in its structure cause cracks to overgrow, provoking it to fracture easily. Hence, different researchers have sought to improve the fracture toughness of alumina through the addition of reinforcing materials in its matrix [2-8]. It has been established that the reinforcement mechanism is due to the deflection of cracks when they move forward and collide with a metallic particle [9-10]. Another critical situation that improves the mechanical characteristics of the alumina is the final grain size in its microstructure so that if it is possible to obtain fine grains at the end of the processing, the properties of the same will be enhanced. There are several suggested methods for making alumina-based composites with good final characteristics. For example, Alweendo et al. comment that the incorporation of submicron SiC into Al_2O_3 matrix improves mechanical properties of the matrix [8]. Winter et al. fabricated nickel-Al_2O_3 composites with compositionally graded microstructures with different physical properties [11]. Konopka and Szafran have produced Al_2O_3-Al composites via infiltration of porous ceramics by liquid Al; they comment in their work that microstructure of obtained composites can be important in applications in which electrical properties of a material are relevant [12]. Davis in his work describes chemical and physical properties of Al_2O_3, as well as its manufacturing process and its applications or uses [13]. Guglielmi et al. establish a methodology to produce full-scale, all-oxide composites with porous reaction-bonded aluminum oxide (RBAO) with good physical properties [14]. Despite the large number of studies carried out to process alumina and improve its physical properties through incorporating different reinforcements, the combination of Reaction Bonded Aluminum Oxide (RBAO) and Spark Plasma Sintering (SPS) processes for obtaining alumina has not been reported. The RBAO is based on homogeneously mixed powders containing 40% to 60% of aluminum combined with alumina; during an oxidation treatment (usually in an oxygen atmosphere) the aluminum is oxidized to

[1] UNIVERSIDAD POLITÉCNICA DE VICTORIA, CIUDAD VICTORIA, MÉXICO

* Corresponding author: erochar@upv.edu.mx

γ-Al_2O_3 at a temperature of approximately 900°C and undergoes a phase transformation to α-Al_2O_3 at 1100°C. The alumina obtained by this method has better physical characteristics than the one obtained by other methods, and it can even have nanometric sizes [15-17]. On the other hand, it is well known that through the SPS process, it is possible to retain the very fine particle size of the powder after sintering, which can be explained due to the very high speeds of the method for consolidating materials [18-19]. In this work, alumina-based composite reinforced with silver or titanium pure metals were manufactured by means of the combination of RBAO and SPS process, aimed to determine the effect of these metals on the mechanical, electrical and optical properties of the resulting composites.

2. Experimental details

Alumina-based composites were fabricated from Al_2O_3 powder (Sigma-Aldrich, 99.9%, 5 μm); metals powders employed were Ag and Ti, both (Mayer, 99.5%, 1 μm). The amount added of the corresponding metal was 0.5 and 3 vol.%. The amounts of metals used were chosen because, in previous similar works, alumina-based composites with this amount of metals were those that yielded the best fracture toughness values [20-21].

The processing of the desired composite materials was carried out in two stages. In the first stage, alumina and 40% aluminum were intensively dry-mixed in air in a planetary mill (Retsch PM 100, Germany). The powders resulting from this grinding were subjected to a heating cycle at 1°C/min up to 1,100°C and keeping the powder there for 1 hour to achieve the oxidation of the aluminum according to reaction 1 (RBAO process, in an electrical furnace Carbolite RHF17/3E). A sample of these powders was subjected to TGA analysis to follow aluminum oxidation progress (Shymadzu, DTG60H). Once the alumina was obtained through the RBAO process, it was intensively mixed with silver or titanium powders. The grinding and mixing of the powders were carried out for 3 hours at a rotation speed of 300 rpm, using a stainless steel container with zirconia grinding elements of 0.3 cm diameter, the ratio between powder weight/balls weight was 1:10, grinding was carried out using 3 ml of isopropyl alcohol as a control medium. The resulting powders from the second milling stage were consolidated by plasma spark sintering (Dr. Sinter SPS-1020), heated at a rate of 100°C/min up to 900°C for 5 min in vacuum; a sintering pressure of 30 MPa was applied. The particle size distribution of milled powders was determined using a Mastersizer 2000 equipment of English origin. The density was determined by the alcohol immersion method based on Archimedes' principle, as is specified in ASTM C20-00 [22]. Before characterization of the sintered samples, all of them were prepared to mirror finish SiC papers grinding and polishing using 3 μm and 1 μm diamond suspension. Observations of the microstructure of each sintered sample were performed by optical microscopy (Nikon, Eclipse MA 200, Japan). The ultrasonic method determined Young's modulus, following the ASTM C1198 – 09 standards [23], using a Grindosonic A-360 Japanese manufacturing equipment. Microhardness was evaluated in agreement with the ASTM C1327 standards [24]. In this case, twelve measurements were performed at different sample locations; these measurements were performed with a microhardness tester (Wilson Instruments Model S400, Japan). The fracture toughness was determined by the indentation fracture method using Miyoshi's equation [25].

$$2Al + 3/2O_2 \rightarrow Al_2O_3 \tag{1}$$

$$K_{IC} = 0.018\left(\frac{E}{H}\right)^{0.5}\left(\frac{P}{c^{1.5}}\right) \tag{2}$$

Where: K_{IC} is the fracture toughness ($MPam^{0.5}$), H is the Vickers hardness (GPa), E is the modulus of elasticity (GPa), P is the applied load (N), and c is the average length of the cracks obtained from the Vickers fingerprint tips (m). Electrical characterization was performed to sample's pellets as follows; electrical resistivity was obtained by Kelvin's method, also known as four-point method. Capacitors with a material's sample as dielectric were constructed. Dielectric constant was determined utilizing sample's dimensions and capacitance measurements. Regarding measurements of the optical properties, samples of the manufactured pellets were pulverized. A suspension of 24 mg of powder in 10 ml of distilled water was prepared for each material. Suspensions were measured in a quartz cuvette with a CCD spectrometer (Thorlabs, NJ, CCS200) and a quartz tungsten-halogen lamp (Thorlabs, NJ, QTH10) with broadband emission from 400 to 2200 nm. Absorbance measurements were carried out by using an integration time of 500 ms in all the samples.

3. Results and discussion

3.1. Powder sizes (aluminum + alumina)

Fig. 1 shows the curve of cumulative (%) vs. particle size, also in this figure it is presented the curve of Vol (%) vs. particle size (first milling stage). In these curves it is possible to observe that a good distribution of particle sizes is obtained in the powders after the grinding stage. The cumulative (%) versus particle size graph in the figure indicates that 50% of the powders contain particle sizes of less than 1.5 microns; another 30% of the powders have sizes of approximately 2 microns; the remaining 20% of the powders are between 2 and 2.5 microns. On the other hand, the Vol (%) vs. particle size curve shows the homogeneous size distribution of the particles since in the sample, there are particles with sizes ranging from 0.3 microns to particles of about 2.5 microns. This particle size distribution obtained after the grinding step favors the consolidation of the material, besides significantly helping in the aluminum oxidation reaction through the RBAO process, fulfilling one of the main objectives of this project. Also, these results indicate that the grinding stage was effective in obtaining fine particles, which will help ensure a good development in the sintering phase because the multiple contacts between the particles will favor the diffusion processes.

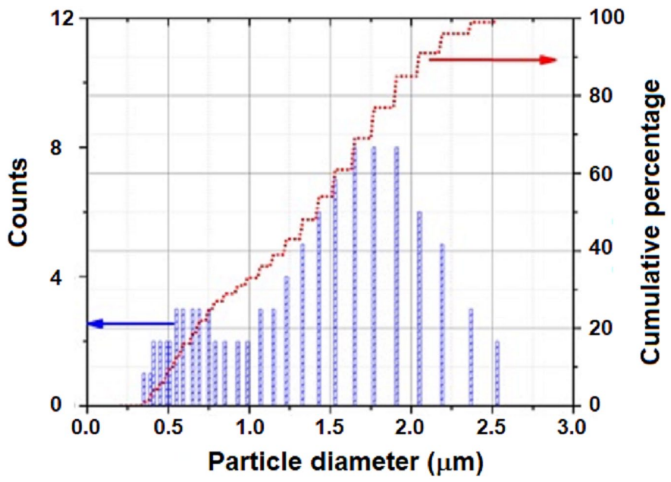

Fig. 1. Particle size analysis graph of powders after milling

3.2. Thermogravimetric analysis (RBAO process)

Fig. 2 shows the thermogravimetric analysis carried out on the mixture of Al + Al_2O_3 powders subjected to the heating cycle used to form alumina through the oxidation of aluminum (RBAO process). The graph shows that from room temperature and up to 500°C, the weight of the sample remains constant; from 500°C, there is a slight weight gain which ends at 650°C; at higher temperatures, the weight gain is more significant, this weight gain ends at approximately 900°C. Both weight gains are related to the oxidation of aluminum according to reaction 1. By observing the temperatures at which this gain in weight occurs, the aluminum has to oxidize slightly when it is in a solid state, and subsequently, its oxidation is stronger when it is in a liquid state. The total weight gain was approximately 11% which corresponds to the amount of oxygen that entered the mixture as mentioned above to oxidize the aluminum and form the new alumina. This gain in weight corresponds well with the stoichiometric amount of aluminum oxidized during

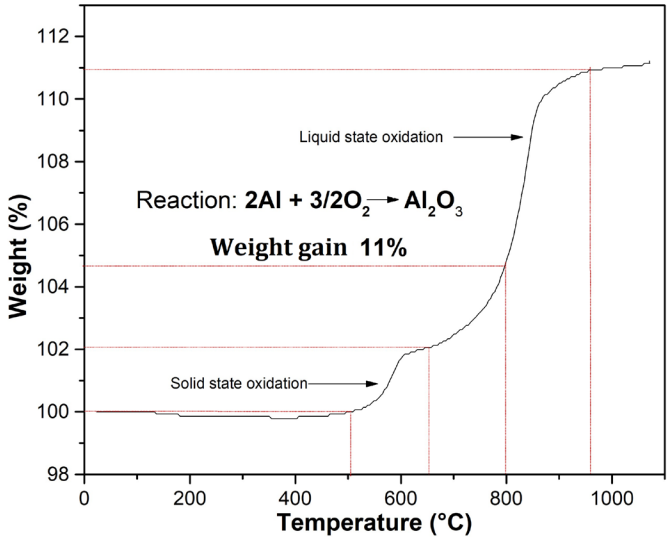

Fig. 2. Thermogravimetric analysis of Al + Al_2O_3 mixture powders heated at 1,100°C

the RBAO process step. Another important situation to note is that aluminum oxidizes more when it is in liquid phase than when it is solid; the reason for this is that there is a greater area of contact with oxygen and greater diffusion of oxygen in the metal. This behavior was also documented by Claussen et al. when he proposed the RBAO technique [15].

3.3. XRD evolution of RBAO process

Fig. 3 presents the X-ray diffraction patterns obtained from interrupted tests at different temperatures during the oxidation cycle, which was done in order to observe the progress of the aluminum oxidation reaction (RBAO process). These diffraction patterns corroborate what was observed in the thermogravimetric analysis since they show that the intensity of the aluminum peaks decreases as the temperature increases, while the intensity of the alumina peaks increases. This behavior indicates that reaction 1 is taking place, which is completed when the sample reaches 900°C, because at this temperature, there is no longer a peak corresponding to aluminum. This response is also observed in the work of Claussen et al. [15].

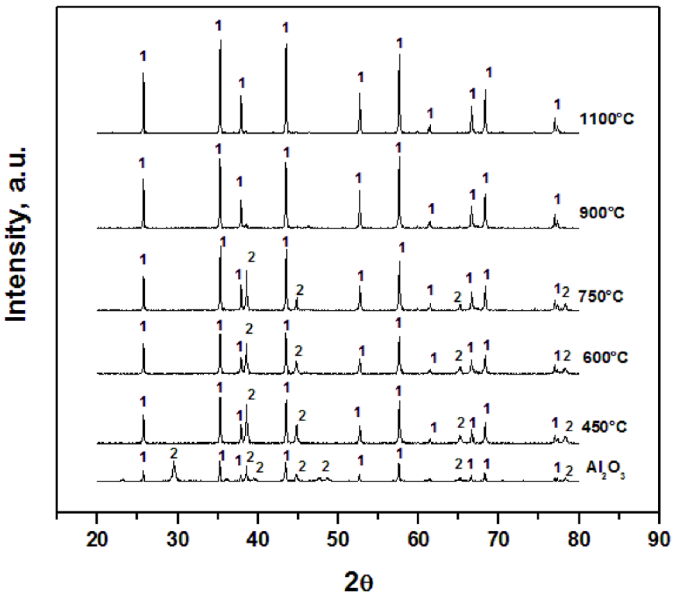

Fig. 3. X-ray diffraction patterns of interrupted tests at different temperatures during the oxidation cycle. 1: Al_2O_3, 2: Al

3.4. XRD sintered samples

Fig. 4 presents the X-ray diffraction patterns obtained on the sintered samples by spark plasma; the lower part of the figure corresponds to the control´s sample (no metal was added). This pattern shows the presence of peaks corresponding to the alumina. The following two patterns correspond to the samples to which silver was added, where, in addition to the peaks corresponding to alumina, several low-intensity peaks corresponding to silver can be distinguished. The two patterns at the top of the figure correspond to the sample with titanium additions;

some low-intensity peaks can be identified in these patterns, corresponding to titanium. The low intensity of the silver and titanium peaks in the respective pattern is explained by the fact that the additions of these metals in the samples were minimal. However, the most important thing about this figure is that it is verified that the desired composition was obtained at the end of the sintering stage since no other crystalline species corresponding to another material are observed.

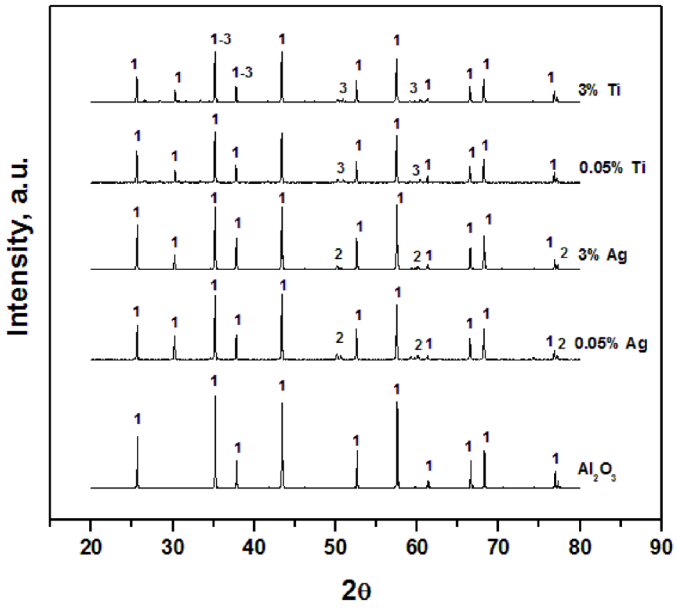

Fig. 4. X-ray diffraction patterns of the sintered samples by spark plasma. 1: Al_2O_3, 2: Ag, 3: Ti

In order to corroborate the presence of silver and titanium in the composites, X-ray energy dispersive analysis (EDS) was performed on the corresponding composite. Fig. 5 shows the spectra obtained from this analysis. The analysis was performed on the light and dark phases of the microstructures presented here. In the spectrum of Fig. 5a, the dark phase of the microstructure shows the presence of the chemical elements Al and O, which correspond to the alumina matrix of the sample. When the same analysis is performed on the clear phase of the same microstructure, it can be observed that in the spectrum, in addition to the elements Al and O, peaks appear that correspond to the silver added to the composite. Identical observations are made when the EDS analysis is performed on the sample with titanium additions. Fig. 5b shows that the spectrum obtained from the dark phase analysis indicates the presence of Al and O, while the spectrum obtained from the light phase analysis shows the presence of titanium. These analyses confirm the XRD results, which indicate the formation of the Al_2O_3-Ag and Al_2O_3-Ti composites.

3.5. Microstructure

Fig. 6 presents the micrographs obtained by optical microscopy of the sintered samples; in general, dense and homogeneous

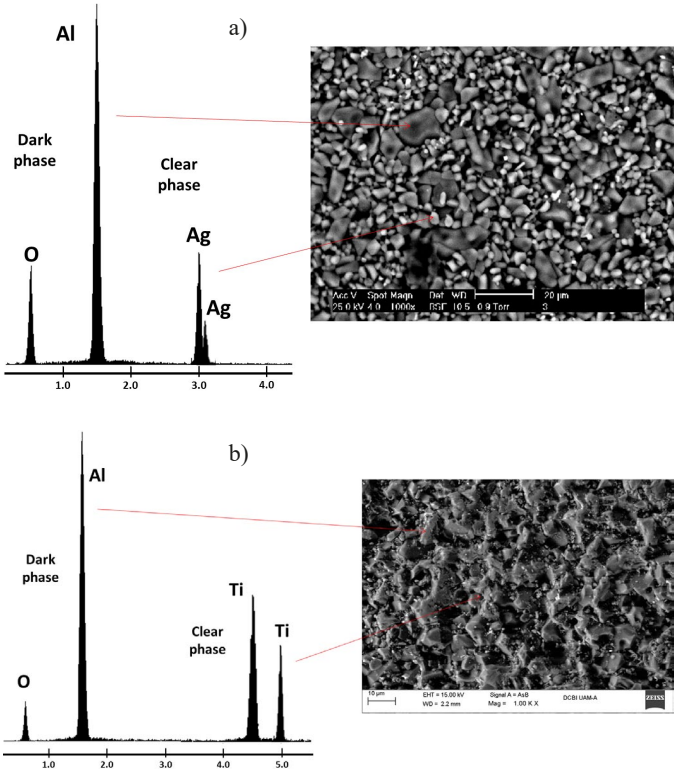

Fig. 5. Spectra of the EDS analysis performed in (a) Al_2O_3-Ag and (b) Al_2O_3-Ti composites

microstructures are observed in these pictures. The microstructure is so fine that neither the grain boundaries nor the added metals presence can be observed, except for the pure alumina sample; in this case, some pores and defects are observed. In the other samples, neither the presence of porosity nor defects in the samples are observed. Therefore, it can be considered that the samples were adequately sintered.

3.6. Mechanical properties

Fig. 7 presents the relative densities and elastic modulus of the sintered samples; concerning density, the pure alumina sample was the one that reached the lowest degree of density, having obtained 96% of its relative density. When silver is added to alumina, its relative density improves up to 97%, while when titanium is added, the relative density reached was 98%. From these results, it is clear that additions of metals that are good conductors of heat accelerate the diffusion of atoms during sintering which is reflected in bodies better densified. As far as the elastic modulus is concerned, the opposite effect occurs because with metals' addition, the modulus of the resulting composite decreases. This effect is normal because metals are much less rigid or, in other words, have less elastic modulus than alumina, so that when combining alumina with metal, the elastic modulus decreases. On the other hand, no significant effect of the metal content on the final elastic modulus of the composite is observed since the final modulus was similar for the two metal contents studied. Ighodaro and Okoli, in their

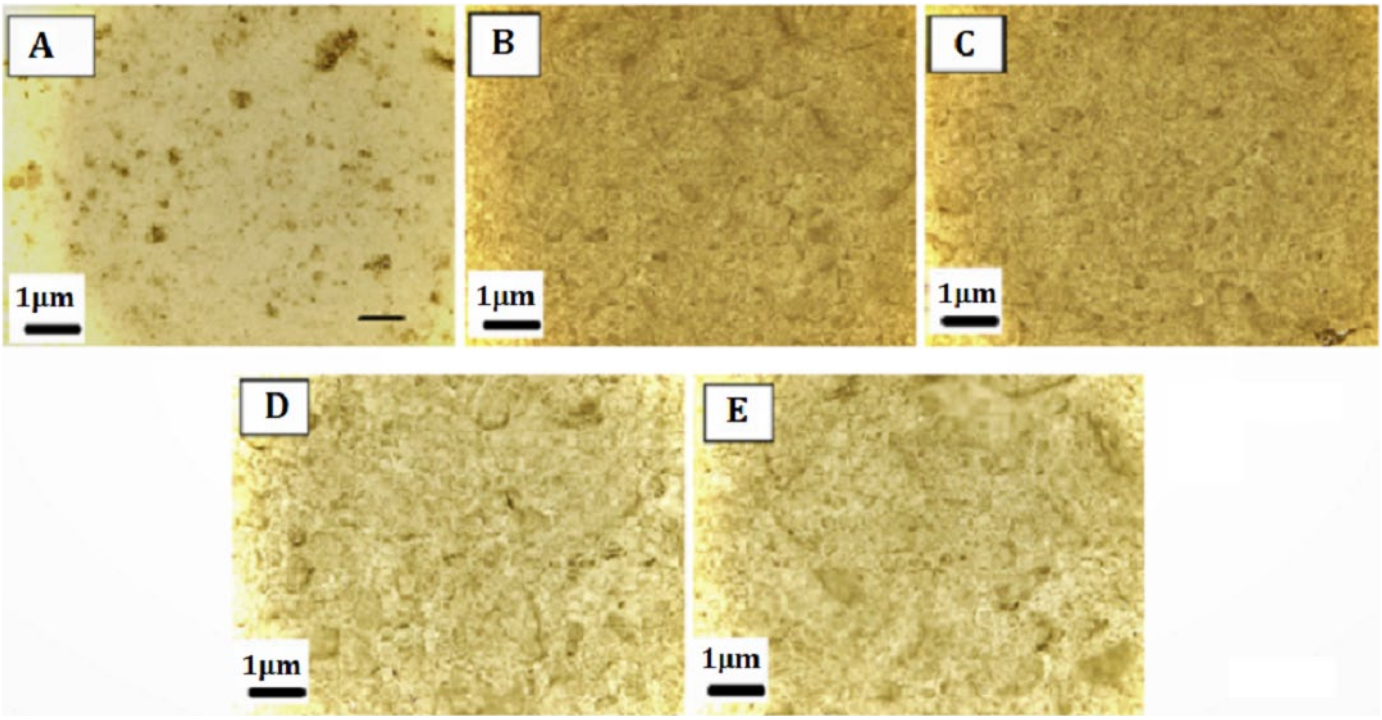

Fig. 6. Optical microscopy micrographs of the sintered samples. A: Al_2O_3, B: Al_2O_3-0.05%Ag, C: Al_2O_3-3.0%Ag, D: Al_2O_3-0.05%Ti, E: Al_2O_3-3.0%Ti

review, report several works where alumina was reinforced with different metals in which elastic moduli similar to those of this work were obtained [9].

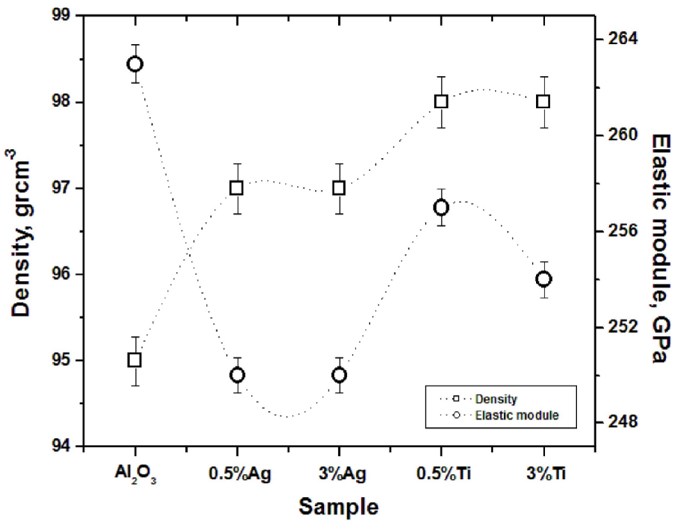

Fig. 7. Relative densities and elastic modulus of sintered samples

Fig. 8 presents the values of hardness and fracture toughness of the sintered samples; as concerns the hardness of the samples, it is to be expected that the sample with the highest hardness was the one containing 100% alumina. However, with silver additions, the hardness of the composite decreases by up to 30%. On the other hand, the hardness only decreases by 6% for the sample with titanium additions. As in the elastic module, metals are softer than alumina, hence this behavior. However, the better toughness of metal with respect to ceramic is shown in this same figure, as the fracture toughness of alumina is improved by up to 112% for the sample with additions of 0.5 vol.% silver, while, for the composite with additions of 0.5 vol.% titanium fracture toughness increases by 72%, which is also favorable. One reason for these high values of fracture toughness obtained in these composites is the good degree of densification obtained in them, coupled with the presence of very fine structures. The reinforcement mechanism that acts in this type of composite has been well documented [9-10] and reported as the deflection of cracks that collide with metal particles as they grow, and must deviate its trajectory in order to continue growing, which translates into

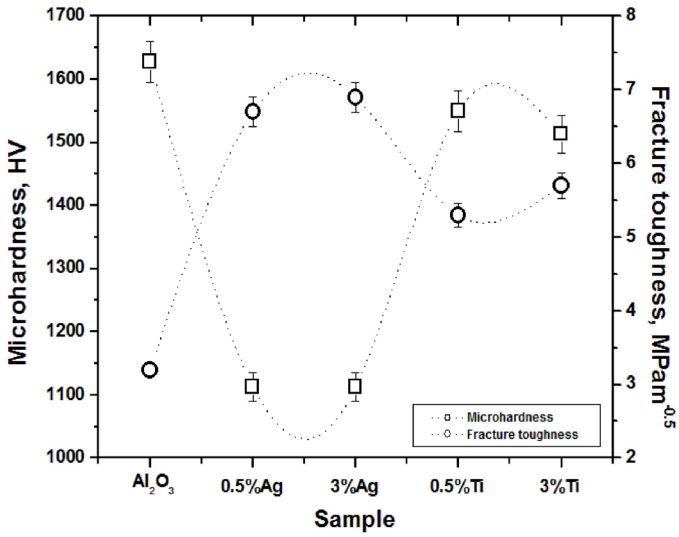

Fig. 8. Hardness and fracture toughness of sintered samples

greater energy consumption and hence an improvement in the toughness of the composite. The results indicate that there is no considerable effect of the different amounts of reinforcing metal used on the hardness or fracture toughness of the composites.

Fig. 9 shows a typical fingerprint resulting from the microhardness test where the cracks formed during indentation can be observed and used to calculate the fracture toughness of the materials under study. It is worth mentioning that the reported result is the average of 12 measurements performed in different indentations.

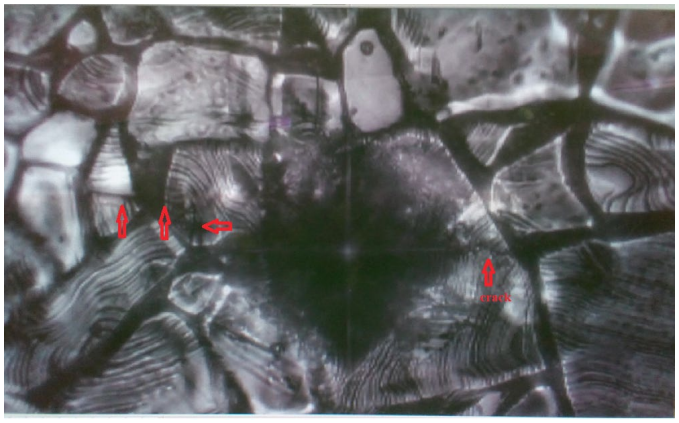

Fig. 9. Typical fingerprint resulting from the microhardness test, used to calculate fracture toughness in composites

3.7. Optical properties

Fig. 10 shows absorbance response in the range from 400 to 800 nm of pure Al_2O_3 and Al_2O_3 with Ag or Ti additions; as can be seen, pure Al_2O_3 shows the lower absorbance in the visible range. It can also be observed two small peaks at 542 and 609 nm; these peaks are enhanced with Ag or Ti additions. It is noticed that Ti additions show a linear increase in the Al_2O_3 absorbance. Regarding Ag additions, a higher absorbance than in Ti is observed for both 0.5 vol.% and 1.0 vol.% additions.

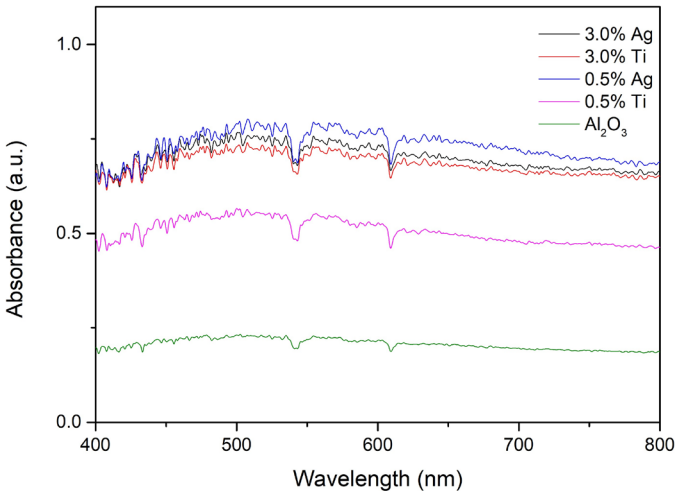

Fig. 10. Visible light absorption of Al_2O_3 and Al_2O_3 with Ag or Ti additions

Light absorption enhancement in the visible range could expand or improve the areas of application of Al_2O_3. For example, Dordevic et al. [26] extended the visible optical absorption of Al_2O_3, increasing the band gap to convert the Al_2O_3 from insulator to semiconductor. Al_2O_3 can also be utilized to improve the performance in perovskite solar cells [27].

3.8. Electrical properties

Fig. 11 shows the electrical properties for the studied materials; the resistivity present in these samples is within a range characteristic of insulating materials, typically from 10^8 to 10^{20} Ωm [28]. However, the addition of silver or titanium to the alumina causes a decrease of 90 and 70% respectively in the resistivity of the alumina, thus losing part of the insulating properties of the alumina. This phenomenon is due to the natural electrical conductive characteristic of metals. Also, in Fig. 11 it can be observed an increase of the dielectric constant depending on the doping material added to alumina, but with values close to that of pure alumina, so the addition of metals to the alumina does not have a significant effect on its dielectric constant.

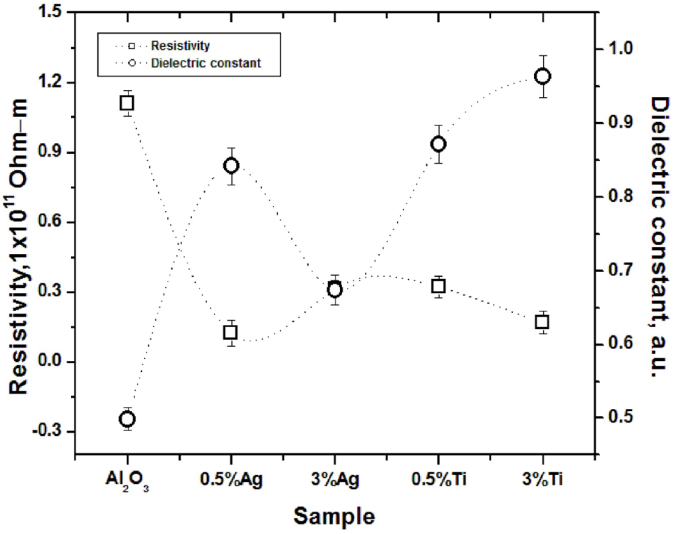

Fig. 11. Resistivity and dielectric constant of sintered samples

4. Conclusions

- Through the combination of the RBAO and SPS processes, it was possible to successfully manufacture dense alumina-based composites reinforced with silver or titanium microparticles. The RBAO process helped obtain fine particles smaller than 1 micron, which favored the consolidation of the samples. Furthermore, the rapid consolidation of the samples during the SPS process helps to retain the fine particle size after the sintering step.
- Of the two amounts of reinforcing metals used (0.5 and 3 vol.%), the results indicate that these amounts are not considerably affected on the different properties evaluated.

On the other hand, the use of silver resulted in increasing the mechanical and electrical properties of alumina, while titanium better absorbs radiation in the visible spectrum.

- The use of reinforcing metals in alumina improves its fracture toughness considerably. An improvement of 112% and 72% was obtained when using 3 vol.% of silver and titanium respectively in the value of this property. The reinforcement mechanism that acts in this type of composite is the deflection of cracks that collide with metal particles as they grow.

Acknowledgments

The authors are grateful to the Department of Mechanical Engineering, Toyohashi University of Technology, Japan for the facilities given to develop the present work.

REFERENCES

[1] A. Shakeel, K. Suvardhan: Handbook of Bionanocomposites, Pan Stanford Publishing Ltd (2018).

[2] M. Szafran, K. Konopka, E. Bobryk, K.J. Kurzydłowski, J. Eur. Ceram. Soc. **27**, 651-654 (2007). DOI: https://doi.org/10.1016/j.jeurceramsoc.2006.04.046

[3] C. Liu, J. Zhang, J. Sun, X. Zhang, Ceram. Int. **33**, 1319-1324 (2007). DOI: https://doi.org/10.1016/j.ceramint.2006.04.014

[4] E. Rocha-Rangel, J. López-Hernández, C.A. Calles-Arriaga, W.J. Pech-Rodríguez, E.N. Armendáriz-Mireles, J.A. Castillo-Robles, J.A. Rodríguez-García, J. Mater. Res. **34**, 1-7 (2019). DOI: https://doi.org/10.1557/jmr.2019.178

[5] Y.N. Li, W.Z. Zhang, Y.F. Cao, T.E. Zhang, Ad. Mater. Res. **853**, 68-72 (2013). DOI: https://doi.org/10.4028/www.scientific.net/AMR.853.68

[6] C. Marci, P. Katarzyna, J. Eur. Ceram. Soc. **27**, 1273-1277 (2007). DOI: https://doi.org/10.1016/j.jeurceramsoc.2006.05.093

[7] K. Wonbaek, O. Hyun-Su, S. In-Jin, Int. J. Refract. H. Met. **48**, 376-381 (2015). DOI: https://doi.org/10.1016/j.ijrmhm.2014.10.011

[8] S.T. Alweendo, O.T. Johnson, B.M. Shongwe, F.P. Kavishe, J.O. Borode, Mat. Res. **23**, 1-9 (2020). DOI: https://doi.org/10.1590/1980-5373-mr-2019-0363

[9] O.L. Ighodaro, O.I. Okoli, Int. J. Appl. Ceram. Technol. 313-323 (2008). DOI: https://doi.org/10.1111/j.1744-7402.2008.02224.x

[10] P. Agrawal, C.T. Sun, Compos. Sci. Technol. **64**, 1167-1178 (2004). DOI: https://doi.org/10.1016/j.compscitech.2003.09.026

[11] A.N. Winter, B.A. Corff, I.E. Reimanis, B.H. Rabin, J. Amer. Ceram. Soc. **83**, 2147-2154 (2000). DOI: https://doi.org/10.1111/J.1151-2916.2000.TB01528.X

[12] K. Konopka, M. Szafran, J. Mater. Proc. Technol. **175**, 266-270 (2006). DOI: https://doi.org/10.1016/j.jmatprotec.2005.04.046

[13] K. Davis, Material review: Alumina (Al_2O_3). School of Doctoral Studies (European Union) Journal 109-113 (2010).

[14] P.O. Guglielmi, D.E. Garcıa, M.P. Hablitzel, D. Blaese, D.P. Goulart, A. Borchert, R. Janssen, J. Ceram. Sci. Technol. **7**, 87-96 (2016). DOI: https://doi.org/10.4416/JCST2015-00038

[15] N. Claussen, S. Wu, D. Holz, J. Eur. Ceram. Soc. **14**, 97-109 (1994). DOI: https://doi.org/10.1016/0955-2219(94)90097-3

[16] H.K. Lee, Korean J. Mater. Res. **23**, 574-579 (2013). DOI: http://dx.doi.org/10.3740/MRSK.2013.23.10.574

[17] H.K. Lee, HK, Korean J. Mater. Res. **25**, 215-220 (2015). DOI: http://dx.doi.org/10.3740/MRSK.2015.25.5.215

[18] B.N. Kim, K. Hiraga, K. Morita, H. Yoshida, Scr. Mater. **57**, 607-610 (2007). DOI: https://doi.org/10.1016/j.scriptamat.2007.06.009

[19] A. Teber, F. Schoenstein, F. Têtard, M. Abdellaoui, N. Jouini, Int. J. Refract. H. Met. **30**, 64-70 (2012). DOI: https://doi.org/10.1016/j.ijrmhm.2011.06.013

[20] S.J. Esparza-Vázquez, ScM thesis, Reinforcement of alumina-based ceramics (Al_2O_3) with titanium (Ti) nanoparticles, Politechnic University of Victory, México (2014).

[21] A. Pérez-de la Fuente, Alumina-Silver Composites Manufacturing, Politechnic University of Victory, México (2015).

[22] ASTM: Standard test methods for apparent porosity, water absorption, apparent specific gravity, and bulk density of burned refractory brick and shapes by boiling water. C20-00 (2010).

[23] ASTM standard test method for dynamic Young's modulus, Shear modulus, and Poisson's ratio for advanced ceramics by sonic resonance. C1198-09 (2013).

[24] ASTM standard test method for Vickers indentation hardness of advanced ceramics. C1327 (2015).

[25] T. Miyoshi, N. Sagawa, T. Sassa, T. Jpn. Soc. Mech. Eng. Ser. **A51**, 2489-2497 (1985). DOI: https://doi.org/10.1299/kikaia.51.2489

[26] V. Đorđević, D.N. Sredojević, J. Dostanić, D. Lončarević, S.P. Ahrenkiel, N. Švrakić, E. Brothers, M. Belić, J.M. Nedeljković, Micropor. Mesopor. Mat. **273**, 41-49 (2019). DOI: https://doi.org/10.1016/j.micromeso.2018.06.053

[27] H. Si, Q. Liao, Z. Zhang, Y. Li, X. Yang, G. Zhang, Z. Kang, Y. Zhang, Nano Energy. **22**, 223-231 (2016). DOI: https://doi.org/10.1016/j.nanoen.2016.02.025

[28] R.E. Hummel, Electrical Properties of Materials. In: Understanding Materials Science. Springer, New York, NY (1998). DOI: https://doi.org/10.1007/978-1-4757-2972-6_11